separations

MDPI

Article

Removal of Sr(II) in Aqueous Solutions Using Magnetic Crayfish Shell Biochar

Wenchao Lu [1,2,3], Jundong Feng [4], Marta Otero [5], Tao Liao [1,2,3,*] and Liang Qiu [1,3,4,5,*]

1 Institute of Agro-Products Processing and Nuclear Agricultural Technology, Hubei Academy of Agricultural Sciences, Wuhan 430064, China; wenchaolu@haac.com
2 School of Chemistry and Environmental Engineering, Wuhan Institute of Technology, Wuhan 430000, China
3 Key Laboratory of Cold Chain Logistics Technology for Agro-Product, Ministry of Agriculture and Rural Affairs, Wuhan 430064, China
4 Department of Materials Science and Technology, Nanjing University of Aeronautics and Astronautics, Nanjing 210016, China
5 CESAM, Department of Environment and Planning, Campus Universitário de Santiago, 3810-193 Aveiro, Portugal
* Correspondence: liaotao0728@hbaas.com (T.L.); qiuliangyzl@126.com (L.Q.)

Abstract: The cooling water of nuclear power plants and discarded crayfish shells (CS), both containing Sr(II), are waste resources that cause environmental pollution and endanger human health. In this study, magnetic biochar produced by crayfish shells (mag@CSBC) was used as an adsorbent to remove radionuclide Sr(II) in an aqueous solution and under irradiation conditions. Scanning electron microscopy, X-ray diffraction analysis, Fourier-transform infrared spectroscopy and vibration sample magnetometer analysis were used to characterize mag@CSBC. In addition, an isothermal adsorption experiment conducted under irradiation conditions determined that the maximum adsorption capacity of mag@CSBC was 21.902 mg/g, which was 1.896 mg/g higher than that from experiments conducted under conditions without irradiation and more suitable for the Freundlich isotherm model. The kinetic experiment proved that irradiation could improve the adsorption cap acity of mag@CSBC and reduce the adsorption equilibrium time. At the same time, the experiment further proved that, under irradiated conditions, the adsorption rate of mag@CSBC can reach more than 90%, and the adsorption capacity is the highest when the pH is 8 and the reaction process is exothermic. Competitive adsorption with Na(I) has a high selectivity and strong recyclability. Finally, the mechanism of Sr(II) adsorption by mag@CSBC under irradiation was studied. In conclusion, mag@CSBC, as a low-cost, easy-to-synthesize, environmentally friendly and easy-to-recycle adsorbent, can be applied in batches for the removal of Sr(II) in aqueous solutions. In particular, the concept of using irradiation technology to optimize adsorption behavior serves as an inspiration for future research.

Keywords: biochar; adsorption; strontium

check for updates

Citation: Lu, W.; Feng, J.; Otero, M.; Liao, T.; Qiu, L. Removal of Sr(II) in Aqueous Solutions Using Magnetic Crayfish Shell Biochar. *Separations* **2023**, *10*, 310. https://doi.org/10.3390/separations10050310

Academic Editor: Mohamed F. Attallah

Received: 22 March 2023
Revised: 3 May 2023
Accepted: 8 May 2023
Published: 13 May 2023

Copyright: © 2023 by the authors. Licensee MDPI, Basel, Switzerland. This article is an open access article distributed under the terms and conditions of the Creative Commons Attribution (CC BY) license (https://creativecommons.org/licenses/by/4.0/).

1. Introduction

Strontium is widely found in soil and seawater and is an essential trace element in the human body. Its chemical structure is similar to Ca(II) [1], and it can protect the human heart against myocardial ischemia/reperfusion injury and prevent arteriosclerosis and thrombosis [2]. At the same time, Sr-90 is also one of the most abundant radionuclides in the cooling water of nuclear power plants, with a half-life lasting as long as 29 years [3]. After being absorbed by human body, Sr is easily accumulated in the liver, lungs and kidneys [4], damaging the genetic material in cells and leading to bone cancer and nervous system diseases [5,6]. Therefore, the highly selective removal of Sr(II) from aqueous solutions is of great significance to environmental resources and human health.

Crayfish are native to South America and now widely distributed across over 50 countries and regions, such as the US, Britain, Australia and China; they have become one of the most widely distributed aquatic products, with the largest output of any aquatic product [7]. Studies have shown that crayfish shells (CS) are an integral part of crayfish. However, in actual production, they are mostly treated as biological waste, and only a few are sold as low-value raw materials [8]. Discarded CS cause mosquitoes and flies to wreak havoc and spread diseases, produce malodorous gases, pollute water and affect human health [9]. Especially in recent years, due to the COVID-19 pandemic, crayfish have mostly been sold as cold-chain shrimp tails; the output of CS has increased, and its distribution has become more concentrated [10]. In addition, biochar (BC) has a large surface area and large pore size, playing an important role in removing metal ions from wastewater [11–15]. Meanwhile, crayfish shell biochar (CSBC) contains a variety of chemical groups (carboxyl, hydroxyl, amino, etc.) [16–18], indicating that it has a unique application potential as an adsorbent. Thus, converting waste CS into BC can not only alleviate disposal problems but also create a valuable adsorbent to adsorb Sr(II) and address the challenges of energy shortage, environmental crises and increasing customer demand [19].

At present, there are various methods and techniques for the separation and removal of Sr, such as the use of alkyd resins [20], mesoporous silica [21,22] and activated carbon (AC) [23], etc. However, synthesizing these adsorbents is expensive and time-consuming. Recently, research has been conducted on the low-cost and easy synthesis of materials containing Sr(II) adsorbents, such as pecan shell, paprika biochar, banana peels biochar, basil seed, coffee grounds and bamboo charcoal [24–29]. However, experiments using CSBC, especially mag@CSBC magnetized by magnetite, to adsorb Sr(II) have not yet been carried out. Moreover, the Sr(II) adsorption behavior of magnetic adsorbents under irradiated conditions is still unknown. Gamma rays have a large initial adsorption energy and are capable of carrying out rapid and uniform reactions at room temperature [30,31]. Compared with chemical, ultraviolet or plasma methods, gamma rays can produce a large number of free radicals, reduce the bond energy of adsorption and enhance the grafting process [32]. Therefore, after achieving the easy recovery of mag@CSBC via magnetization, we carried out an innovative exploration of methods to improve the adsorption capacity of an adsorbent via irradiation technology.

In this study, mag@CSBC was synthesized from CS, which can effectively remove radionuclide Sr(II) from an aqueous solution and has the advantage of a high recovery after adsorption. In addition, the physical and chemical properties of the adsorbent were determined using scanning electron microscopy (SEM), X-ray diffraction (XRD), Fourier-transform infrared spectroscopy (FTIR) and a vibrating sample magnetometer (VSM). Considering the isotherm model, kinetic model, adsorbent dosage, pH value, temperature, coexisting Na(I) ions and desorption and re-adsorption experiments, the adsorption behavior and regeneration availability of mag@CSBC were evaluated, and the mechanism of adsorption of Sr(II) by mag@CSBC under irradiation conditions was clarified.

2. Experimental Section

2.1. Materials

The crayfish shells used in this study came from a market (Wuhan, China). All used chemicals and reagents were of analytical grades. Strontium nitrate ($Sr(NO_3)_2$, 99.5%) as a simulated solution was purchased from Sinopharm Chemical Reagent Co., Ltd. (Beijing, China). For synthesizing mag@CSBC, ferric chloride hexahydrate ($FeCl_3 \cdot 6H_2O$, 99%), ferrous sulfate heptahydrate ($FeSO_4 \cdot 7H_2O$, 99%), and ammonia solution (NH_4OH, 30%) were purchased from Sinopharm Chemical Reagent Co., Ltd. (Beijing, China). To study the effect of pH and sodium chloride, salt, nitric acid (HNO_3, 65%), sodium hydroxide (NaOH, 25%), and sodium chloride (NaCl, extra pure) were purchased from Sinopharm Chemical Reagent Co., Ltd. (Shanghai, China). All the solutions were prepared using deionized (DI) water (Direct-Q$^{@}$5UV, ERCK MILLIPORE, Darmstadt, Germany).

2.2. mag@CSBC

The CS were washed with ultrapure water and dried in an oven at 60 °C. The dried CS were incinerated in a 600 °C muffle furnace for 2 h. The temperature was increased to 200°C in the first stage, and then a heating rate of 50 °C/min was maintained for 10 min. In the second stage, the heating rate was 5 °C/min, and the temperature was raised to 400 °C for 1 h. The heating rate in the third stage was 1 °C/min, and the temperature was maintained at 600 °C for 2 h. The biochar was kept under a continuous stream of N for 2 h to ensure a constant temperature, and the flow rate of N was 0.1 m^3/h. Finally, biochar was crushed and passed through 100-mesh sieves and used as an adsorbent crayfish shell biochar (CSBC). The mag@CSBC was prepared as follows. First, 26.62 mg $FeCl_3 \cdot 6H_2O$ and 55.54 mg $FeSO_4 \cdot 7H_2O$ were added to 100 mL of ultrapure water. Then, 1g of the CSBC was dispersed in the solution and stirred for 48 h at room temperature. Thereafter, the solution was adjusted to pH 10 using NaOH and reacted for 24 h at 80 °C. Finally, to obtain mag@CSBC, the CSBCs were washed 2–3 times with distilled water and dried overnight in an oven at 60 °C.

2.3. Characterization

The element composition of the adsorbent was determined using an elemental analyzer of FLASH2000 (Thermo Scientific, Waltham, MA, USA). The specific surface area and pore properties were measured using an ASAP2460 instrument (Mack, Greensboro, NC, USA) and the N_2 adsorption–desorption curve, and calculated via Barrett–Joyner–Harenda (BJH) analysis. Adsorbent morphologies were analyzed using a platinum target and Schottky field emission SEM (TESCAN, Brno, Czechia). A D8 advanced X-ray diffractometer (Bruker, Billerica, MA, Germany) equipped with a Cu Kα radiation source (λ = 0.15406 nm at 40 kV and 40 mA) was used to analyze the crystalline phase of the powder samples. Additionally, the FTIR spectrum of the samples was tested using a Nicolet iS20 spectrometer (Thermo Electron, Waltham, MA, USA) over a range of 400~4000 cm^{-1}. Finally, the magnetic moments of adsorbents were calculated using VSM analysis (LakeShore7404, Columbus, OH, USA).

2.4. Adsorption Experiments

All the adsorption experiments were performed three times in 15 mL conical tubes (PE, HaiMen China). Except for the adsorbent dosage experiments, the 10 mL Sr(II) analog solution was treated with 20 mg of the adsorbent. All the irradiated experiments were completed in the Hubei Agricultural Products Irradiation Center, using ^{60}Co-ray with an activity of 1.18×10^{16} Bq. The adsorption time was 30 h, and the dose of irradiation was 4000 Gy [33,34].

2.4.1. Adsorption Isotherms and Kinetics

To investigate the effect of the initial concentration of Sr(II), 20 mg of the adsorbent was used for an Sr(II) solution at different initial concentrations (10, 20, 30, 40, 50, 60, 70, 80 and 100 mg/L) and adsorbed at 120 rpm for 22 h. Kinetic experiments were performed using a 70 mg/L Sr(II) solution with sampling intervals of up to 2 h.

2.4.2. Effect of Dosage, pH, Temperature and Na(I)

Furthermore, to investigate the effect of the dosage, the amount of added adsorbent was set to 10, 20, 30, 40, and 50 mg/L for adsorption. To investigate the effect of pH, 70 ppm of Sr(II) was adjusted to a different initial pH (4, 6 and 8) using 0.1 mol/L of HNO_3 and NaOH solution. To investigate the effect of temperature, the reaction temperatures were set at 25, 35, 45, 55 and 65 °C in 70 mg/L concentrations for isothermal adsorption. All of the above experiments were performed using mag@CSBC in an irradiated environment. In addition, we investigated the effects of Na(I) using 10,100 and 1000 mg/L NaCl and 60, 70 and 80 mg/L Sr(II) solutions.

2.4.3. Adsorption-Desorption Experiment

To determine the reuse potential of mag@CSBC, the adsorption–desorption efficiency of Sr(II) was determined via four reutilization experiments. For the regeneration experiments, 70 mg/L of Sr(II) solution was used in an irradiated environment. Desorption was reacted with 0.1 mol/L of nitric acid for 12 h and separated via centrifugation (3000 rpm, 10 min, 20 °C). After the adsorption reaction, all solutions were centrifuged at 3000 rpm for 10 min. The supernatant was filtered with a 0.22 μm syringe filter head (Whatman). The residual concentration of Sr(II) in the solution was determined using an atomic absorption spectrophotometer (TAS-990, China) at 690 nm.

The adsorption capacity of mag@CSBC for Sr(II) (Q_e, mg/g) and the remaining percentage (r, %) of Sr(II) were calculated via Equations (1) and (2), respectively:

$$Q_e = [(C_0 - C_e) \times V]/m \quad (1)$$

$$R = [(C_0 - C_e)/C_0] \times 100\% \quad (2)$$

where C_0 and C_e (mg/L) represent the initial and equilibrium concentrations of Sr(II), respectively. V (L) is the volume of Sr(II) solution, and m (g) indicates the mass of the adsorbent.

3. Results and Discussion

3.1. Characterization

3.1.1. SEM Observation

The morphology of the CSBC and mag@CSBC composites are shown in Figure 1. The figure shows that the surface of CSBC is rough and loose, with regular cracks and voids. The large pore diameter might be due to the elimination of proteins and other impurities adhering on the surface and inside the pores [35]. The pore structures of CSBC appeared to be cracked and collapsed, and the surface was attached by a number of small particles that could be decomposition products of mineral materials and humic substances in the process of pyrolysis [36]. The heterogeneous spherical particles on its surface indicate an amorphous structure of the biomass [37]. Furthermore, its regular honeycomb morphology was observed due to the presence of calcium salts and chitin-containing compounds such as $CaCO_3$. This morphology is commonly observed in crustacean bio-materials such as shrimp and crabs [38]. The above features are conducive to convenient conditions for the adsorption of Sr(II). Furthermore, in mag@CSBC, magnetite was found to attach to CSBC, and the aggregation of spherical particles was observed. The smooth surfaces shown in Figure 1a,b are attached by magnetite, as shown in Figure 1d at 20 k× magnification. The material characteristics of the CSBC and mag@CSBC are shown in Table 1. Both materials maintain more than half of their yield, while mag@CSBC was larger, possibly because Fe_3O_4 was loaded onto its surface. Additionally, the values of N and H decreased with their modification, which may be related to the destruction of organic compounds in CS [39]. In addition, due to some functional groups (-OH, etc.) being covered by Fe_3O_4, the pH value of mag@CSBC increased [40] and the atomic ratio of H/C, O/C decreased [41]. Finally, the results of BET and average pore diameter were also because of the covered Fe_3O_4.

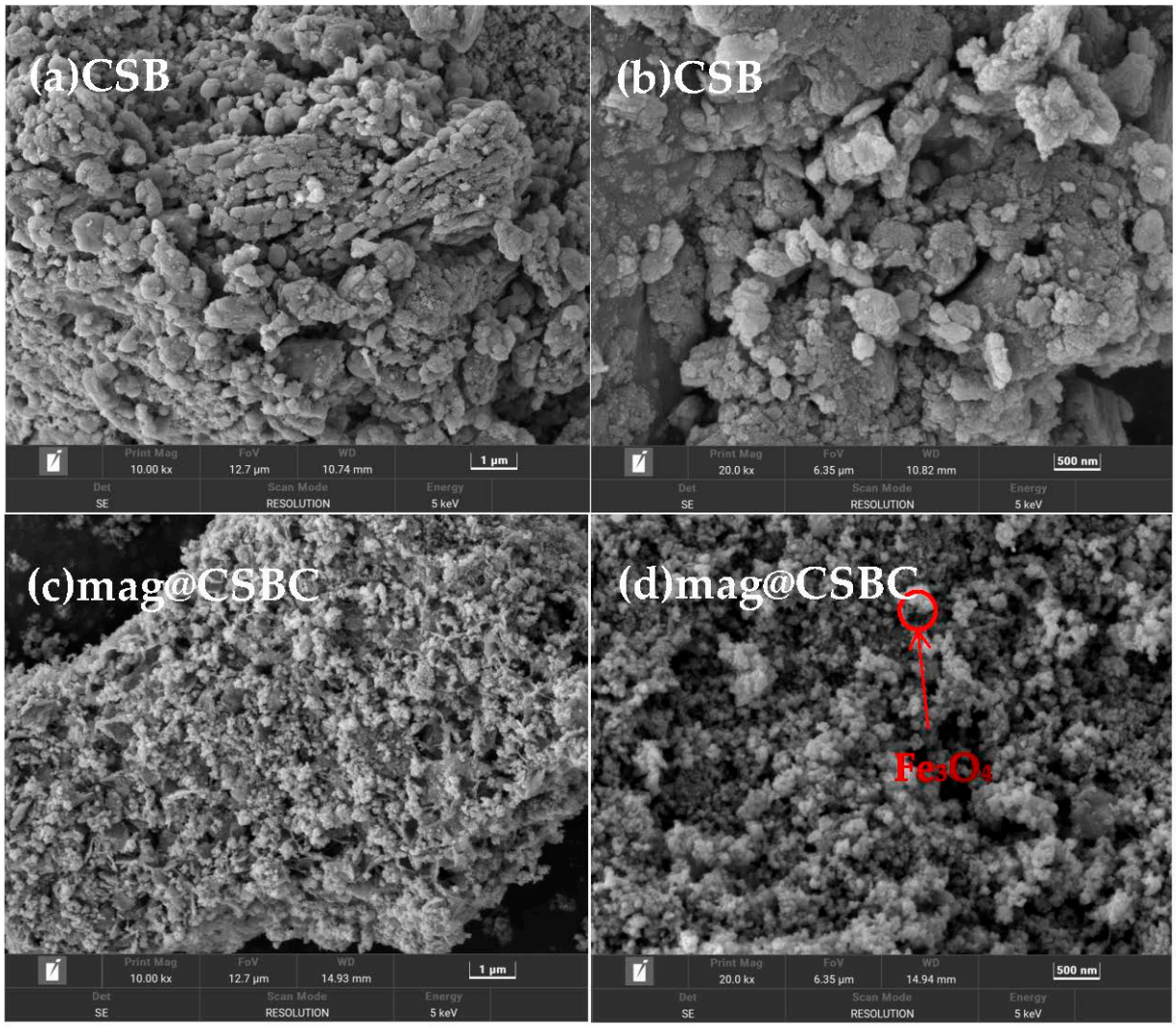


Figure 1. SEM images of (**a**,**b**) CSBC and (**c**,**d**) mag@CSBC.

Table 1. Characteristics of the CSBC and mag@CSBC.

Property	Proportion (CSBC/mag@CSBC)	Property	Proportion (CSBC/mag@CSBC)
Yield (%)	54.53/67.13	Atomic ratio O/C	0.823/0.741
C (%)	18.7/21.22	Atomic ratio H/C	0.33/0.14
N (%)	0.91/0.77	pH value	10.63/9.23
O (%)	20.52/25.13	BET surface area (m^2/g)	26.77/38.12
H (%)	0.52/0.41	Pore volume (cm^3/g)	0.12/0.18
S (%)	2.94/1.32	Average pore diameter (nm)	22.86/14.41
Fe (%)	0/9.43		

3.1.2. XRD Patterns

The Fe_3O_4 peaks were analyzed via an XRD study to confirm that the particles expected to be Fe_3O_4 (Figure 1) represent the actual magnetite. In an XRD pattern (Figure 2), various peaks representing Fe_3O_4 were found in mag@CSBC at 18.002°, 30.166°, 35.533°, 37.129°, 43.15°, 53.45°, 57.005°, 62.735°, 65.854°, 71.005°, 74.051°, and 75.067°, while such peaks

were not found in CSBC. The reduction in solution pH under magnetization conditions promotes dissolution in $CaCO_3$ [42]. Meanwhile, the presence of Mg(II) can also further increase the concentration of solution Ca(II). Thus, mag@CSBC significantly decreased relative to the CSBC at the peak near 30° ($CaCO_3$) [43].

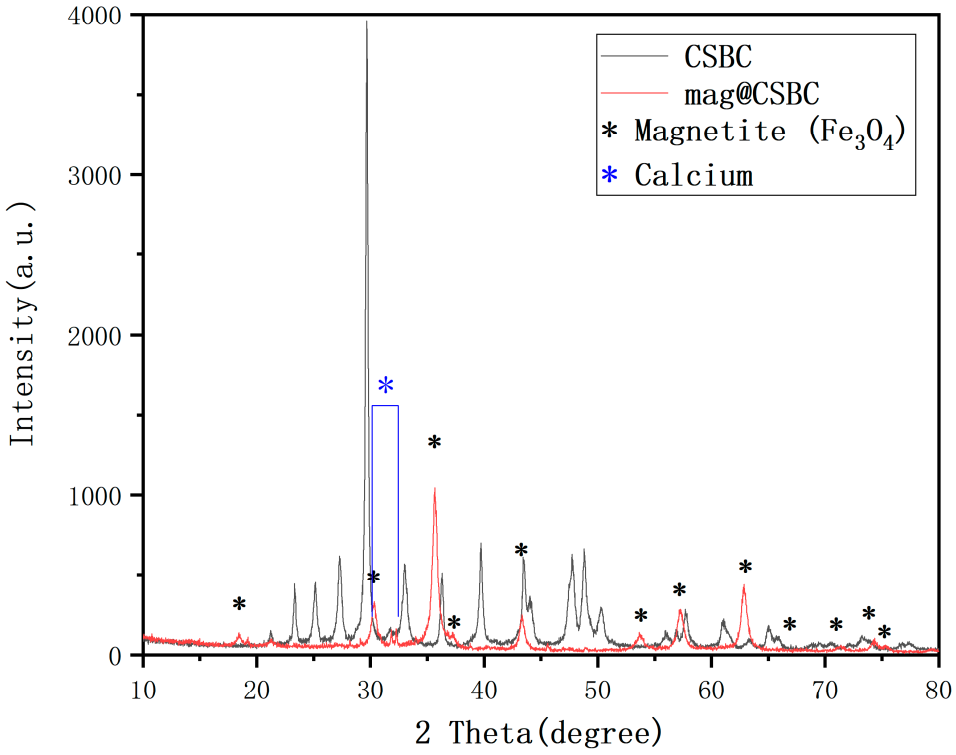


Figure 2. XRD patterns of CSBC and mag@CSBC.

3.1.3. FTIR Spectra

The functional groups of CSBC and mag@CSBC were confirmed via an FTIR analysis (Figure 3). OH bending was observed at 3423.81 cm^{-1}, C-H stretching was 2923.93 (anti-symmetry telescopic vibration peak of CH_2) and a symmetric telescopic vibration peak of CH_3 was observed at 2857.45 cm^{-1} [44]. The C=O, C=C symmetric, and C-O stretching bands were clearly observed at 1795.34, 1622.98 and 1110.61 cm^{-1}, respectively. These results indicate that OH and CO may be a function of proton donors and involved in complexation with Fe [45]. Furthermore, peaks in NH amines groups were observed at 879.34 cm^{-1} [46]. The peaks at 1600 and 1300 cm^{-1} were attributed to the bands of out-of-plane bending, in-plane bending and asymmetric stretching modes of CO_3^{2-} stretching bands, respectively [47]. In the fingerprint region of organic matter, increased C=C stretching suggested an increasing degree of aromatization [48]. Other unique peaks were observed in the spectrum of mag@CSBC, and they were assumed to indicate the reason for the magnetism of CSBC: a peak at 564.53 cm^{-1} implying magnetization with Fe-O [49,50]. Sr(II) adsorption is possible through an electrostatic interaction with highly active functional groups (OH, C-H, C-O, etc.) of CSBC [51]. In particular, the carboxyl and hydroxyl groups present in the CSBC are functional groups that can react with heavy metals in the aqueous phase [52].

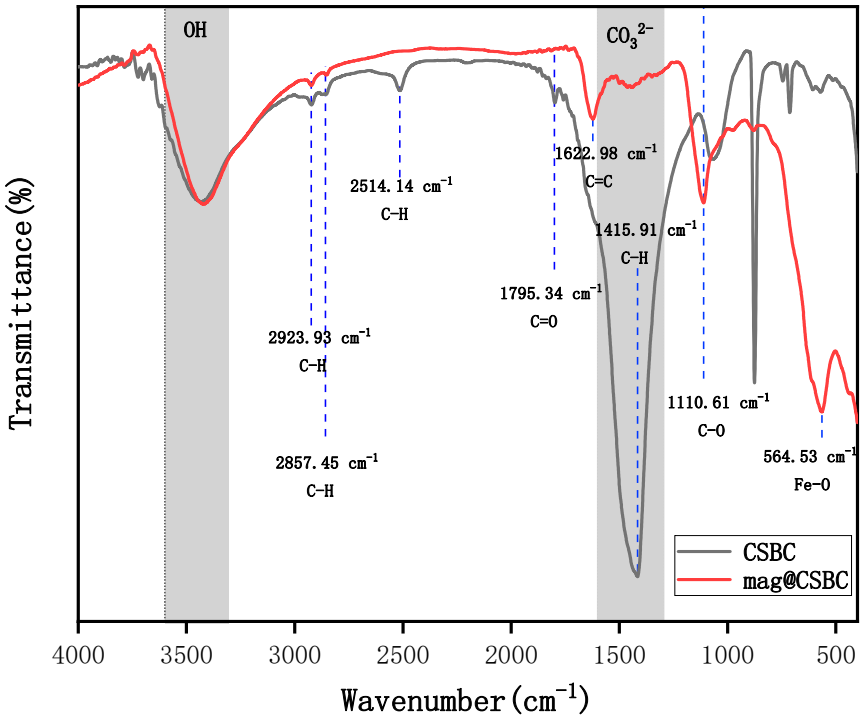


Figure 3. FTIR spectra of CSBC and mag@CSBC.

3.1.4. VSM Analyses

The Fe_3O_4 magnetic strength was analyzed via VSM study to confirm that the particles expected to be Fe_3O_4 (Figure 1) represent the actual magnetite. The intensity of magnetization was confirmed as 49.691 emu/g at room temperature via VSM analysis (Figure 4), indicating greater intensity compared to the previous magnetic adsorbent material [53,54].

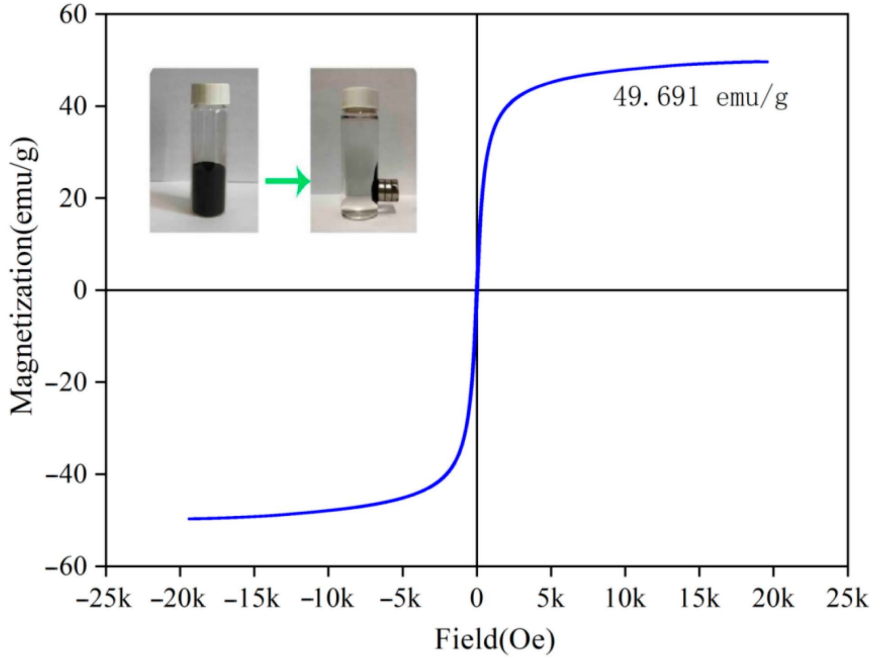


Figure 4. VSM analyses of mag@CSBC.

3.2. Adsorption Experiment

3.2.1. Adsorption Isotherms

The effect of Sr(II) initial concentration on the adsorption capacity of CSBC, mag@CSBC and mag@CSBC-γ (mag@CSBC under an irradiation environment) is shown in Figure 5. The adsorption capacity increases with the increase in the initial concentration of Sr(II). One possible reason is the driving force of initial concentration, which helps to overcome the mass transfer resistance of the adsorbate from adsorbent body to surface.

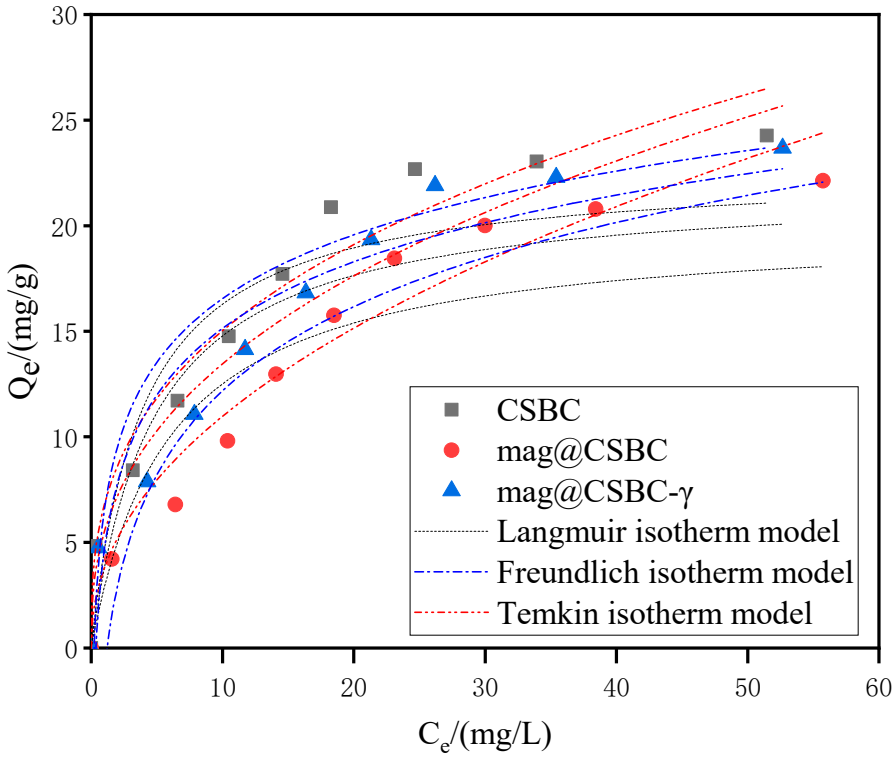


Figure 5. Sr(II) adsorption isotherms of CSBC, mag@CSBC and mag@CSBC-γ (T = 25 °C, pH = 8, Time = 18 H, mag@CSBC = 50 mg/L).

Three types of adsorption isotherm models were used to analyze the equilibrium adsorption behavior: the Langmuir, Freundlich, and Temkin models [55], which are expressed as shown in Equations (3)–(5), respectively:

$$Q_e = \frac{Q_m b C_e}{1 + bC_e} \tag{3}$$

$$Q_e = K_f C_e^{1/n} \tag{4}$$

$$Q_e = \frac{RT}{B} \ln K_T C_e \tag{5}$$

where Q_m is the maximum adsorption capacity of the adsorbent (mg/g) and b is the Langmuir adsorption constant for the free energy of the adsorption (L/mg). Further, K_f [(mg/g) (L/mg)$^{1/n}$] and n are the Freundlich constant and the heterogeneity factor. K_T (L/g), the gas constant R (8.31 J/mol/K), and B (L/mg) are the parameters of the Temkin isotherm.

The fitting effect of the isotherm model was evaluated by using the correlation coefficient (r^2). The results of isothermal adsorption are also shown in Figure 5. The parameters calculated by fitting to the Langmuir, Freundlich, and Temkin models are listed in Table 2.

The nonlinear fitted isotherm model explains the interaction between the adsorbent and the adsorbate.

Table 2. Important parameters of the Langmuir, Freundlich, and Temkin isotherms models for CSBC, mag@CSBC and mag@CSBC-γ.

Models	Parameters	CSBC	mag@CSBC	mag@CSBC-γ
Langmuir isotherm model	Q_m (mg/g)	22.670	20.006	21.902
	b (L/mg)	0.255	0.167	0.207
	r^2	0.916	0.869	0.904
Freundlich isotherm model	K_f [(mg/g) (L/mg)$^{1/n}$]	6.771	3.761	5.498
	n	2.889	2.151	2.573
	r^2	0.964	0.955	0.969
Temkin isotherms model	K_T (L/g)	4.450	2.773	0.831
	B (L/mg)	10.037	10.488	13.243
	r^2	0.927	0.919	0.939

The CSBC itself showed higher adsorption than the mag@CSBC composite. This observation can be interpreted as a reduction in the specific surface area of CSBC by magnetite; furthermore, it indicates that Ca(II) is present in the CSBC and is favorable for ion-exchange mechanisms with Sr(II) [56]. CSBC is a calcium-rich bio-adsorbent and the mag@CSBC covered by the magnetite results in a reduced Ca(II) concentration on the surface. Therefore, it can be interpreted that CSBC is higher in adsorption ability than mag@CSBC. The CSBC and mag@CSBC were the most suitable for the Freundlich isotherm model, with r^2 values of 0.964 and 0.955, respectively. This indicates that the adsorbent surface may be multi-layer adsorption and adsorbate molecules will be adsorbed when they enter the adsorption force field. Because the adsorption force field has a certain spatial range, adsorption can be multi-molecular layer. The adsorption force decreases gradually with the adsorption layer from inside to outside [55]. Additionally, the low heat of adsorption ($B < 20$ J/mol) for the Temkin model confirms that the adsorption process was maybe physical adsorption. The Langmuir model also predicted the maximum adsorption amounts (Q_m) of 22.670 mg/g and 20.006 mg/g for CSBC and mag@CSBC, respectively. According to the adsorption results, even at low initial concentrations, CSBC with a high Q_e value was suitable for Sr(II) adsorption.

However, although though the adsorption capacity decreases when CSBC is magnetized, it is a very inexpensive and readily available biomass, and it has the advantage of reducing the cost of secondary waste treatment by allowing for the easy recovery of the waste adsorbent after adsorption. Notably, the adsorption capacity of mag@CSBC to Sr(II) is significantly enhanced under an irradiation environment, and the Q_m reaches 21.902 mg/g. Especially when the initial concentration is higher or the amount of adsorbent is slightly increased, Q_m comparable to CSBC can be obtained for mag@CSBC-γ. This may be because the irradiation affects the chemical and physical properties of the adsorbent surface, making it highly sensitive to Sr(II), and is conducive to the molecular adsorption on the adsorbent surface [57,58]. Another reason could be that the delocalized electrons of the surface aromatics can move upon irradiation, changing the aromatic molecules with bonded or nonbonded electrons to those with anti-bonded electrons, thus enhancing the contact probability and the adsorption trend [59]. The above is the main reason for irradiation-increased adsorption.

Table 3 lists the Q_m values for Sr(II) adsorption for comparison with the results obtained in studies using other biomass materials. It can be found that the low-cost, environmentally friendly, easy-to-synthesize and reusable adsorbent has become a research hotspot. The Q_m values of carboxymethyl chitosan and coffee grounds are significantly higher than those of mag@CSBC. However, the Q_m values of Hybrid membranes and Paprika biochar are much lower than mag@CSBC. Although the Q_m varies with the types of materials, the reason why this study is worthy of attention is that the raw materials (shrimp shell waste)

used by the adsorbent have the characteristics of putrefaction, stench and environmental pollution. Mag@CSBC activated by magnetite has the advantage of easy separation. In particular, the new viewpoint that γ -ray irradiation can relatively improve the Q_m of adsorbent in the adsorption process will provide new inspiration for related research.

Table 3. Comparison of adsorption capacity of various adsorbents for Sr(II) removal.

Adsorbent	Q_m (mg/g)	References
mag@CSBC-γ	21.902	This study
mag@banana peels biochar	23.827	[26]
carboxymethyl chitosan	105.81	[60]
Fe_3O_4@titanate fibers	37.1	[61]
Melamine-trimesic acid modified attapulgite	26.21	[62]
Paprika biochar	0.02	[25]
Hybrid membranes	0.94	[63]
coffee grounds	69.013	[28]

3.2.2. Adsorption Kinetics

The experimental data were fitted by two kinetic models, namely, the nonlinear pseudo-first-order model (Equation (6)) and pseudo-second-order model (Equation (7)), which have investigated the controlling mechanism of adsorption processes. The pseudo-first-order model assumes that the number of the free adsorption position on the surface of the adsorbent decides the adsorption rate, and the pseudo-second-order model assumes that the square of the number of the free adsorption position on the surface of the adsorbent decides the adsorption rate, mainly controlled by chemical adsorption [64]:

$$\frac{d_{q_t}}{dt} = k_a(Q_e - Q_t) \tag{6}$$

$$\frac{d_{q_t}}{dt} = k_a(Q_e - Q_t) \tag{7}$$

where Q_t and Q_e (mg/g) are the adsorbed amount of mag@CSBC at time t and at equilibrium, respectively. k_a (1/min) is the pseudo-first-order kinetic constant. k_b (g/mg min) is the pseudo-second-order kinetic constant.

The adsorption behavior of Sr(II) by mag@CSBC and mag@CSBC-γ is shown in Figure 6. Parameters of the kinetic experiments and the results are summarized in Table 4. The fitting effect of the kinetics model was evaluated by using the correlation coefficient (r^2).

Table 4. Parameters of the kinetic experiments and the results.

Models	Parameters	mag@CSBC	mag@CSBC-γ
Pseudo-first-order model	Q_e (mg/g)	20.835	23.473
	k_a (min^{-1})	0.145	0.138
	r^2	0.996	0.972
Pseudo-second-order model	Q_e (mg/g)	26.241	30.183
	k_b (min^{-1})	0.005	0.004
	r^2	0.983	0.952

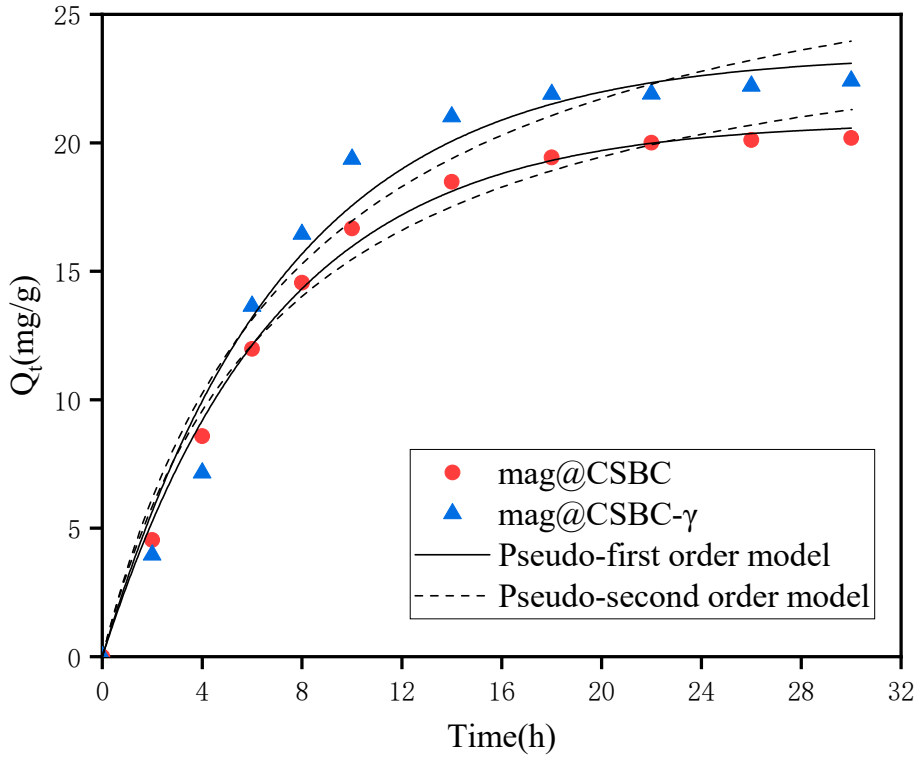


Figure 6. Sr(II) adsorption kinetics of mag@CSBC and mag@CSBC-γ (T = 25 °C, pH = 8, C_0 = 70 mg/L, mag@CSBC = 50 mg/L).

The adsorption of Sr by mag@CSBC almost reached the adsorption equilibrium at 22 h, and the r^2 of the pseudo-first-order model and the pseudo-second-order model were 0.996 and 0.983, respectively. However, under the irradiation condition, the adsorption equilibrium time of mag@CSBC-γ was 18 h, which was 4 h shorter than that under the non-irradiation condition. This indicates that when adsorbing Sr(II) by mag@CSBC, the adsorption equilibrium time can be shortened by irradiation. This may be because the mechanistic reaction of mag@CSBC and Sr(II) grafting copolymerization is triggered by gamma irradiation, which effectively shortens the crosslinking time [65]. The r^2 of the pseudo-first-order model and the pseudo-second-order model are 0.972 and 0.952, respectively. Both of them are more in line with the first-order reaction, and the change of adsorption reaction with time is expected to be proportional to the concentration. The Q_e of mag@CSBC and mag@CSBC-γ under the condition of adsorption equilibrium is 20.835 and 23.473 mg/g, respectively. Furthermore, for mag@CSBC-γ, the isothermal experiment of the adsorption of Sr(II) solution with an initial concentration of 70 mg/L continued to stir for enough time after adsorption for 22 h, and the obtained Q_e (22.114 mg/g) was similar to the kinetic experiment value. Therefore, the results indicate that mag@CSBC quickly reacted with the Sr(II) solution to adsorb Sr(II) under irradiation conditions and confirmed that the stirring time in the isotherm experiment was sufficient.

In addition, the pseudo-first-order model and pseudo-second-order model were fitted with the whole adsorption process, but they could not describe the control step for the different adsorption course. The mechanisms for external mass transfer and intraparticle pore diffusion on the surface were confirmed through the intraparticle diffusion model based on Fick's diffusion law [66]. This can be calculated using the intraparticle diffusion equation, as shown in Equation (8). The rate of intraparticle diffusion equation is obtained as follows:

$$Q_t = k_{di} t^{0.5} + C \quad (8)$$

where k_{di} is the constant of intraparticle diffusion rate [mg/g·min$^{0.5}$]; t is the contact time [min]; C is the constant of intraparticle diffusion [mg/g]; and Q_t is the adsorbed amount at time t [mg/g].

Figure 7 indicates that the mag@CSBC and mag@CSBC-γ adsorbed Sr(II) through three stages: external diffusion (surface diffusion), intraparticle diffusion, and adsorption equilibrium (diffusion within the micropore) [67]. Parameters of the intraparticle diffusion and the results are summarized in Table 5. The fitting effect of the three stages of the intraparticle diffusion model was evaluated by using the correlation coefficient (r^2).

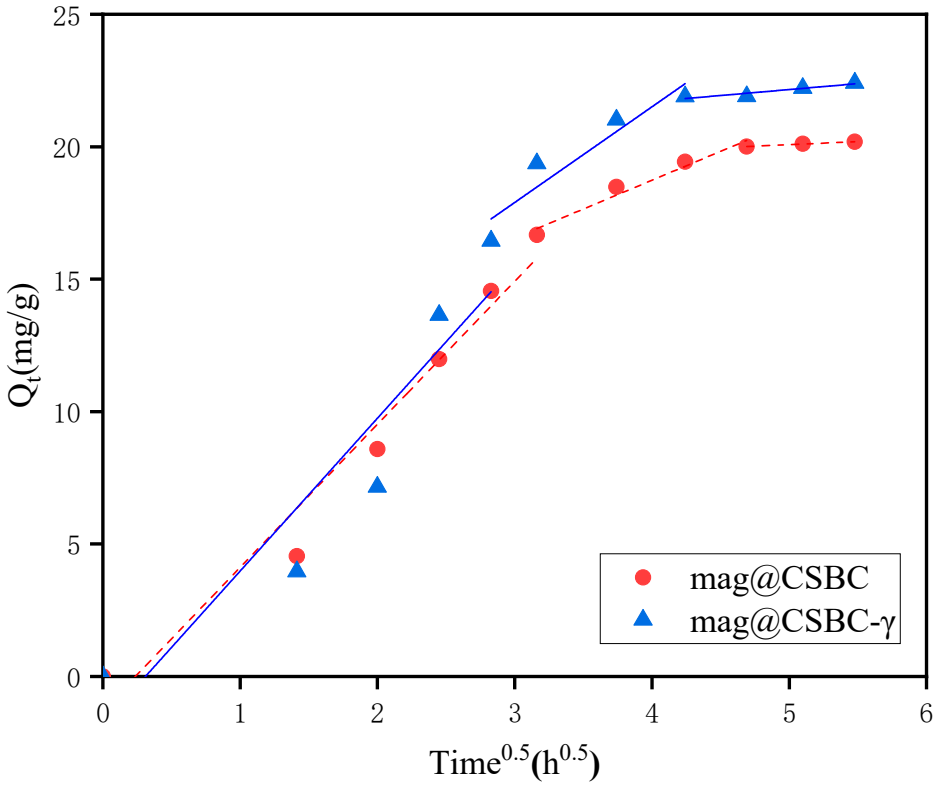


Figure 7. Intraparticle diffusion plot for 70 mg/L of Sr(II) adsorption of mag@CSBC and mag@CSBC-γ (T = 25 °C, pH = 8, mag@CSBC = 50 mg/L, C_0 = 70 mg/L).

Table 5. Parameters of the kinetic experiments and the results under irradiated condition.

Irradiation Environment and Parameter		Adsorption Stage		
		Stage 1	Stage 2	Stage 3
mag@CSBC	k_d (mg/g·min$^{0.5}$)	5.769	2.179	0.230
	C (mg/g)	−1.789	10.020	18.933
	r^2	0.847	0.944	0.984
mag@CSBC-γ	k_d (mg/g·min$^{0.5}$)	6.294	3.612	0.450
	C (mg/g)	−2.341	7.057	19.911
	r^2	0.885	0.834	0.840

The first paragraph indicates the position of the Sr(II) passing across the boundary layer to the outer surface of the mag@CSBC. At this time, k_d is large, indicating that the adsorption occurs rapidly and can be attributed to more adsorption sites on the adsorbent. The second segment indicates that the Sr(II) crosses the outer surface of the mag@CSBC into the pore, at which point the k_d decreases. This may be due to the part of the adsorbent surface site being occupied after the first phase of adsorption. The third segment indicates the adsorption of Sr(II) in the micropores of the inner surface of the mag@CSBC, when k_d is

minimal and the adsorption goes to equilibrium. Furthermore, C not equal to 0 indicates that internal diffusion is not the only rate-limiting step.

3.2.3. Effect of Dosage

The effect of different dosages on the adsorption rate of Sr(II) concentration in the solution is shown in Figure 8. When the initial concentration of Sr(II) in the solution is 70 mg/L, the adsorption efficiency of Sr(II) increases with the increasing amount of mag@CSBC. This may be because the surface area of adsorbent increases, and the number of adsorption sites increases accordingly [43]. With the dosage increasing from 20 mg to 50 mg, the adsorption efficiency increased from 41.07% to 91.36%.

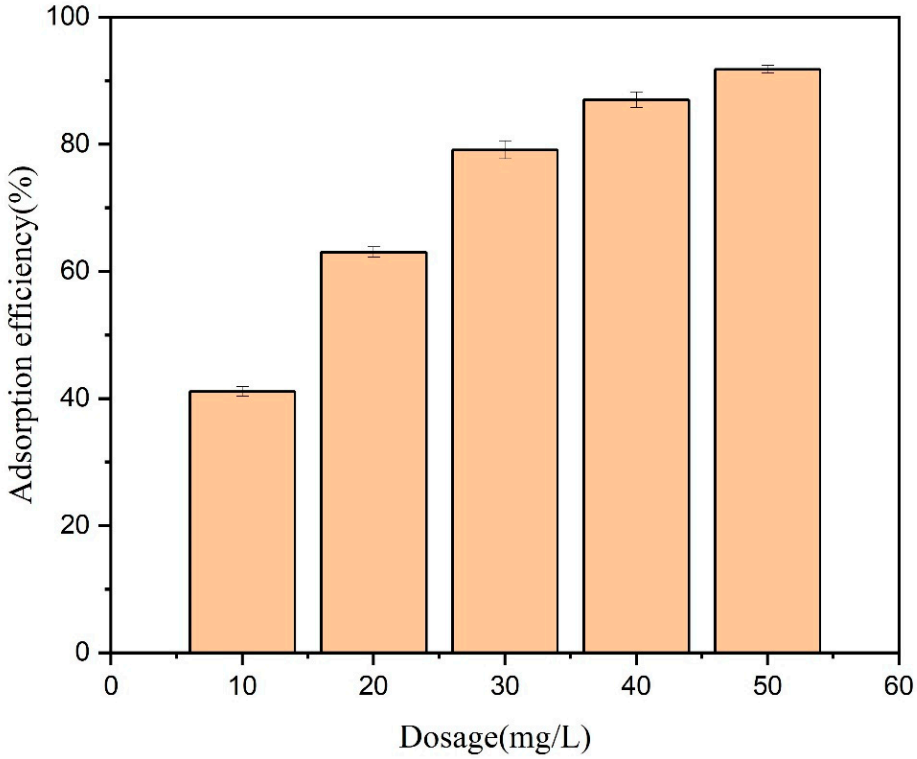


Figure 8. Adsorption efficiency of the different dosage of mag@CSBC (C_0 = 70 mg/L, Time = 18 H, T = 25 °C, pH = 8).

3.2.4. Effect of pH

The effect of different pH levels on the adsorption rate of Sr(II) concentration in the solution is shown in Figure 9. Our results demonstrated that with the increasing of pH, the adsorption efficiency of mag@CSBC for Sr(II) increased. This may because, at low pH, H^+ competes with metal cations for the same adsorption position [68]. When the pH increased, the ability of H^+ to combine adsorption sites decreased, while positively charged strontium ions began to occupy adsorption sites on the surface of the adsorbent and therefore the adsorption capacity increased [69]. However, other studies showed that when the pH increased further (>9), due to the presence of a large number of anions in water, metal ions are surrounded by anions, forming negatively charged atomic groups that reduce the adsorption effect of strontium ions [70,71].

3.2.5. Effect of Temperature

The effect of different temperatures on the adsorption rate of Sr(II) concentration in the solution is shown in Figure 10. It is found that, with the increase in temperature from 25 °C to 65 °C, the adsorption rate of Sr(II) by mag@CSBC gradually decreases. Our results show that temperature has a significant effect on the adsorption of Sr(II) by mag@CSBC. It can be concluded that the adsorption of Sr(II) is an exothermic process.

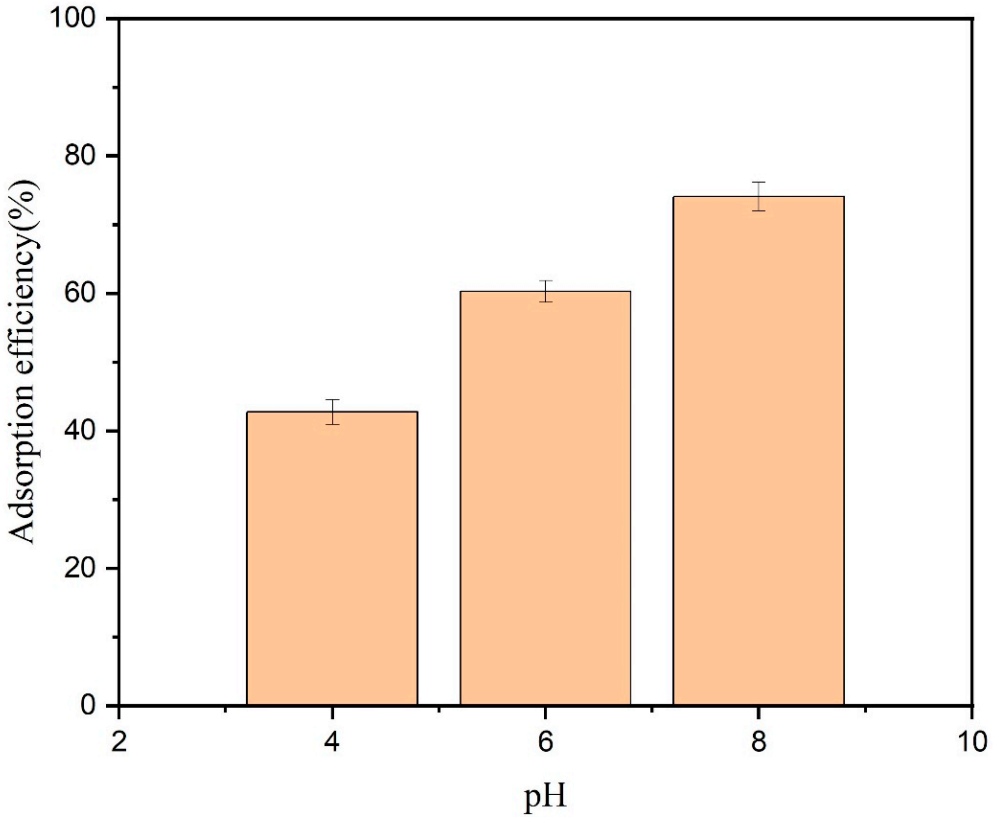


Figure 9. Adsorption efficiency of the different pH of mag@CSBC (C_0 = 70 mg/L, T = 25 °C, mag@CSBC = 50 mg/L, Time = 18 H).

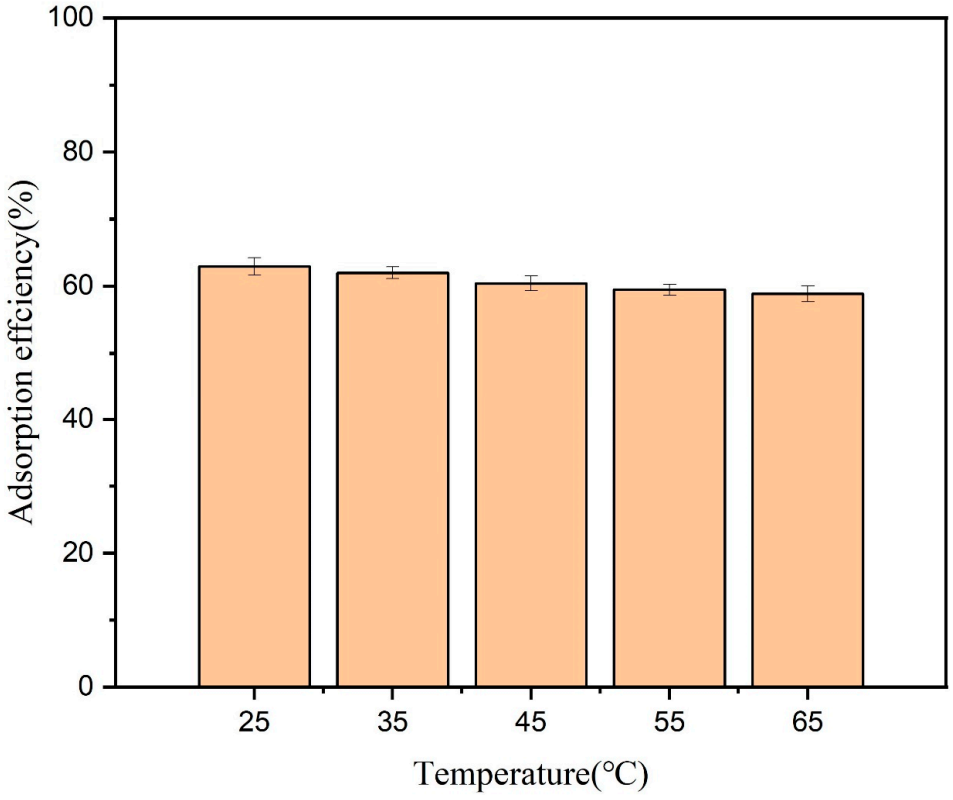


Figure 10. Adsorption efficiency of mag@CSBC at different temperatures (C_0 = 70 mg/L, pH = 8, mag@CSBC = 50 mg/L, Time = 18 H).

3.2.6. Effects of Na(I)

The selective adsorption of Sr(II) in the presence of coexisting ions is influenced by Na(I), Mg(II), and Ca(II) plasma in the wastewater. In particular, Na(I) becomes an important coexisting ion affecting the removal of Sr(II) [26]. Therefore, it is necessary to clarify the effects of Na(I) during Sr(II) adsorption.

To investigate the effect of Sr adsorption during the coexistence of sodium chloride, 60, 70 and 80 mg/L of Sr(II) solution and 10, 100, 1000 mg/L concentrations of sodium chloride were chosen. As shown in Figure 11, under the influence of a coexisting ion of Na(I), the adsorption rate decreases the most with the increase in Na(I) concentration. This phenomenon was most evident in the coexistence of 60 mg/L of the Sr(II) solution and 1000 mg/L of sodium chloride. At the same time, the adsorption rate was found to be less than 50% only when 80 mg/L of Sr(II) solution and 1000 mg/L of sodium chloride coexist, but this problem can be solved by increasing the adsorbent dose. In addition, Formula (1) shows that, with the increase in Sr(II) concentration, Q_e is worth increasing but is still lower than the Q_e value in isotherm experiments, which indicates that Na(I) may undergo competitive adsorption with Sr(II) to seize the adsorption site on mag@CSBC. Nevertheless, mag@CSBC, with its ease of magnetic separation, still has significant advantages for removing the radionuclide Sr(II) present in seawater.

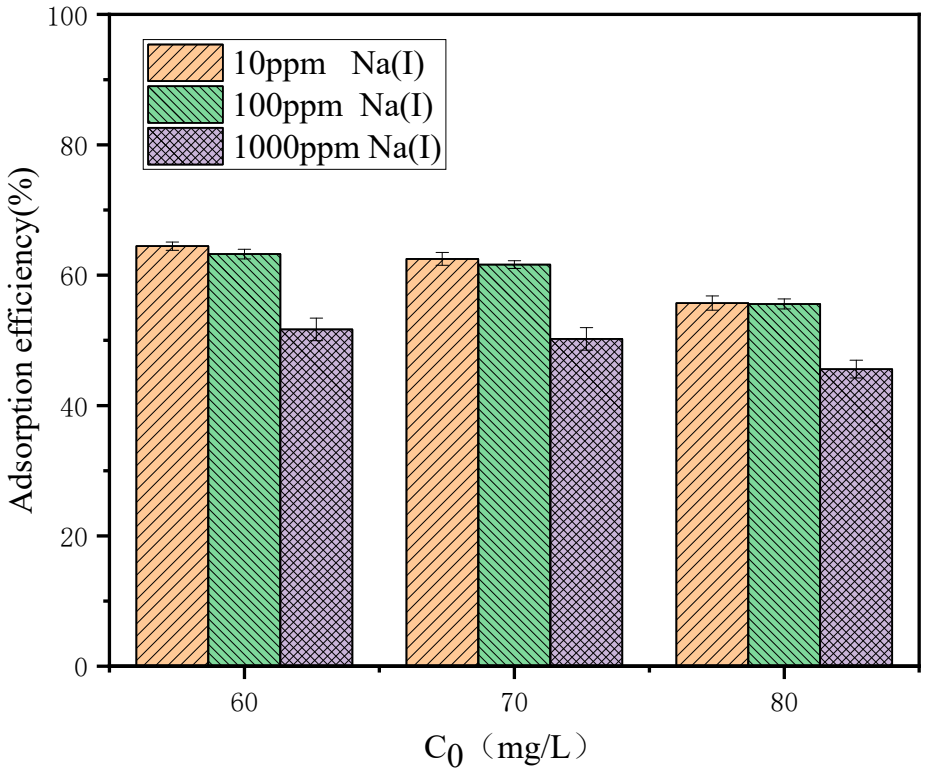


Figure 11. Effect of Na(I) on the efficiency of Sr(II) adsorption by mag@CSBC (pH = 8, mag@CSBC = 50 mg/L, Time = 18 H, T = 25 °C).

3.2.7. Adsorption–Desorption

To determine the reuse efficiency of mag@CSBC under irradiation conditions, the adsorption–desorption efficiency of mag@CSBC was analyzed in four experiments. The experimental results show that the adsorbent recovery is higher than 97%, indicating that the magnetism is well-protected by the layer-covered structure, and the adsorption–desorption efficiency is shown in Figure 12. The results show that the adsorption–desorption efficiency decreased with the number of repeats. However, the adsorption–desorption efficiency of the first three repeats was higher than 50%, and the efficiency was not less than 50% until the fourth reuse of desorption. At the same time, the experiment also proved that

the absorbed Sr(II) is approximately equal to the absorbed concentration of Sr(II), which shows that almost all of the adsorbed Sr(II) can be released by desorption, which once again confirms the possibility of reusing mag@CSBC.

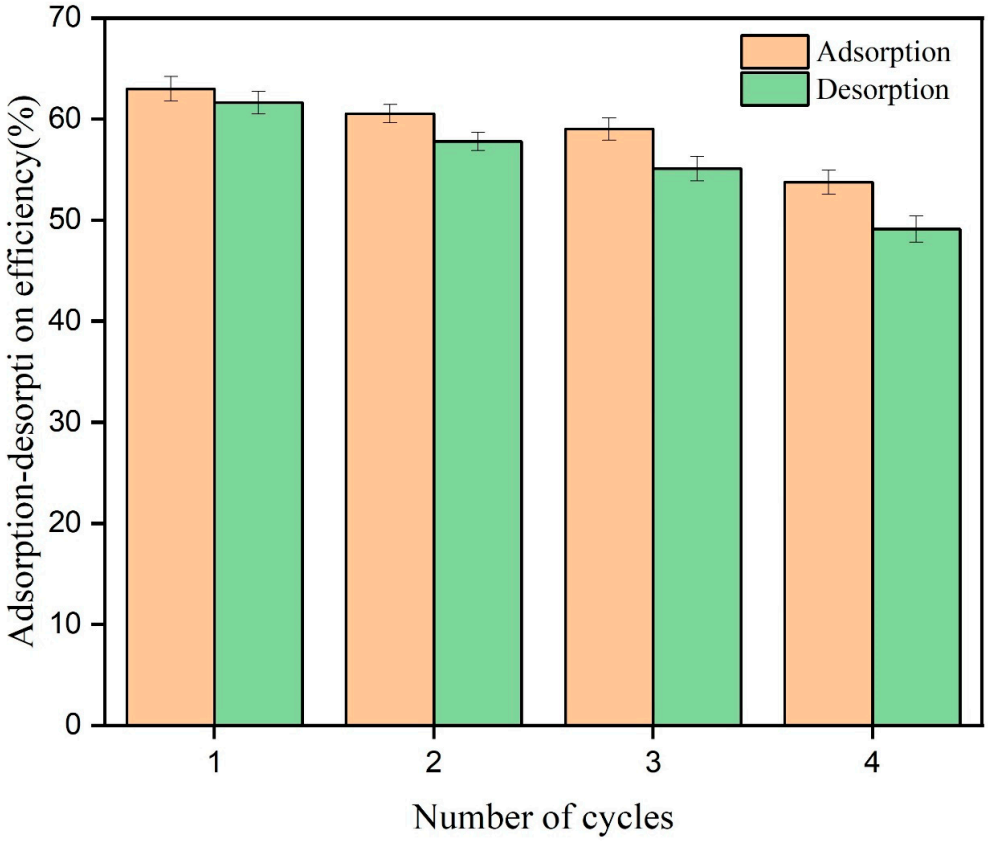


Figure 12. Adsorption and desorption of mag@CSBC composites (C_0 = 70 mg/L, pH = 8, mag@CSBC = 50 mg/L, Time = 18 H, T = 25 °C).

3.3. Mechanism

The mag@CSBC surface is a multilayer of adsorption, and Sr(II) is adsorbed when entering the adsorption force field. Because the adsorption force field has a certain spatial range, the adsorption can be multi-molecular layer. Sr(II) successively enters the adsorbent through surface diffusion, coarse pore diffusion and microdiffusion in the pores. The first stage is mainly the position of Sr(II) through the boundary layer to the outer surface of mag@CSBC. Due to the greater number of adsorption sites on the adsorbent, adsorption rapidly occurs. In the second stage, Sr(II) crosses the outer surface of the mag@CSBC into the pore, which slows down due to part of the site being occupied after the first adsorption phase. In the third stage, the Sr(II) adsorption in the micropores on the inner surface of the mag@CSBC is counterbalanced. In addition, the adsorbent surface functional groups and ions become involved in the adsorption behavior. Particularly under irradiation conditions, the chemical properties and physical properties of the adsorbent surface change, making it highly sensitive to Sr(II), which is conducive to the adsorption of molecules on the adsorbent surface. Meanwhile, the delocalized electrons of the aromatic hydrocarbon on the mag@CSBC surface can move upon irradiation, transforming the aromatic molecules with bonded or non-bonded electrons into those with anti-bonded electrons, thus improving the contact probability and adsorption trend [72].

4. Conclusions

Mag@CSBC, as a low-cost, easily synthesized, environmentally friendly and easily recycled adsorbent, can be widely applied in batches to remove Sr(II) in aqueous solutions.

Meanwhile, gamma radiation irradiation technology can effectively improve the adsorption capacity of mag@CSBC and shorten the adsorption balance time. In this study, the unique physical structure and chemical properties of mag@CSBC composites were verified, proving that the magnetic strength of mag@CSBC is 49.691 emu/g, the maximum adsorption capacity is 21.902 mg/g, the adsorption rate can reach more than 90% and the highest adsorption capacity is at pH 8. The reaction process with Na(I) competitive adsorption has a high selectivity with a strong recovery. Finally, the mechanism of Sr(II) was analyzed via surface diffusion, coarse pore diffusion and inner pore microdiffusion, and this process is accompanied by the influence of adsorbent functional groups and ion exchange (Ca(II), etc.). In this study, we clarified the basic principle of irradiation technology affecting adsorption behavior by increasing the sensitivity of the adsorbent surface to Sr(II) and improving the contact probability and adsorption trend.

Author Contributions: Methodology, W.L.; Investigation, J.F. and M.O.; Writing—review and editing, L.Q.; Funding acquisition, T.L. All authors have read and agreed to the published version of the manuscript.

Funding: This study was supported in part by Key R&D Program of Guangzhou City (202103000087); Young scholars of Hubei Academy of Agricultural Sciences, 2023NKYJJ23; Open Project of Irradiation Preservation Key Laboratory of Sichuan Province, Sichuan Institute of Atomic Energy (FZBZ2022001).

Institutional Review Board Statement: Not applicable.

Informed Consent Statement: Not applicable.

Data Availability Statement: Not applicable.

Conflicts of Interest: The authors declare that they have no competing interest.

References

1. Nitzsche, K.N.; Wakaki, S.; Yamashita, K.; Shin, K.; Kato, Y.; Kamauchi, H.; Tayasu, I. Calcium and strontium stable isotopes reveal similar behaviors of essential Ca and nonessential Sr in stream food webs. *Ecosphere* **2022**, *13*, e3921. [CrossRef]
2. Xing, M.; Jiang, Y.; Bi, W.; Gao, L.; Zhou, Y.-L.; Rao, S.-L.; Ma, L.-L.; Zhang, Z.-W.; Yang, H.-T.; Chang, J. Strontium ions protect hearts against myocardial ischemia/reperfusion injury. *Sci. Adv.* **2021**, *7*, eabe0726. [CrossRef]
3. Hu, B.; Qiu, M.; Hu, Q.; Sun, Y.; Sheng, G.; Hu, J.; Ma, J. Decontamination of Sr(II) on Magnetic Polyaniline/Graphene Oxide Composites: Evidence from Experimental, Spectroscopic, and Modeling Investigation. *ACS Sustain. Chem. Eng.* **2017**, *5*, 6924–6931. [CrossRef]
4. Lalhmunsiama; Tiwari, D.; Lee, S.-M. Physico-chemical studies in the removal of Sr(II) from aqueous solutions using activated sericite. *J. Environ. Radioact.* **2015**, *147*, 76–84. [CrossRef]
5. Boyer, A.; Ning, P.; Killey, D.; Klukas, M.; Rowan, D.; Simpson, A.J.; Passeport, E. Strontium adsorption and desorption in wetlands: Role of organic matter functional groups and environmental implications. *Water Res.* **2018**, *133*, 27–36. [CrossRef] [PubMed]
6. Höllriegl, V.; München, H.Z. Strontium in the environment and possible human health effects. *Encycl. Environ. Health* **2011**, *5*, 268–275.
7. Martín-Torrijos, L.; Martínez-Ríos, M.; Casabella-Herrero, G.; Adams, S.B.; Jackson, C.R.; Diéguez-Uribeondo, J. Tracing the origin of the crayfish plague pathogen, Aphanomyces astaci, to the Southeastern United States. *Sci. Rep.* **2021**, *11*, 9332. [CrossRef] [PubMed]
8. Tang, C.; Xu, Y.; Yu, D.; Xia, W. Label-free quantification proteomics reveals potential proteins associated with the freshness status of crayfish (*Procambarus clarkii*) as affected by cooking. *Food Res. Int.* **2022**, *160*, 111717. [CrossRef]
9. He, C.; Lin, H.; Dai, L.; Qiu, R.; Tang, Y.; Wang, Y.; Duan, P.-G.; Ok, Y.S. Waste shrimp shell-derived hydrochar as an emergent material for methyl orange removal in aqueous solutions. *Environ. Int.* **2019**, *134–143*, 105340. [CrossRef]
10. Bloomer, C.C.; Taylor, C.A.; Distefano, R.J. Integrating burrowing crayfish and waterfowl conservation management on moist-soil wetlands. *Environ. Conserv.* **2022**, *49*, 130–135. [CrossRef]
11. Khan, I.; Saeed, K.; Khan, I.J. Nanoparticles: Properties, applications and toxicities. *Arab. J. Chem.* **2019**, *12*, 908–931. [CrossRef]
12. Lehmann, J.; Kleber, M. The contentious nature of soil organic matter. *Nature* **2015**, *528*, 60–68. [CrossRef] [PubMed]
13. Li, H.; Dong, X.; da Silva, E.B.; de Oliveira, L.M.; Chen, Y.; Ma, L.Q. Mechanisms of metal sorption by biochars: Biochar characteristics and modifications. *Chemosphere* **2017**, *178*, 466–478. [CrossRef] [PubMed]
14. Nansubuga, I.; Banadda, N.; Ronsse, F.; Verstraete, W.; Rabaey, K. Digestion of high rate activated sludge coupled to biochar formation for soil improvement in the tropics. *Water Res.* **2015**, *81*, 216–222. [CrossRef]

15. Woolf, D.; Lehmann, J.; Lee, D.R. Optimal bioenergy power generation for climate change mitigation with or without carbon sequestration. *Nat. Commun.* **2016**, *7*, 13160. [CrossRef] [PubMed]
16. Gao, R.; Xiang, L.; Hu, H.; Fu, Q.; Zhu, J.; Liu, Y.; Huang, G. High effificiency removal capacities and quantitative sorption mechanisms of Pb by oxidized rape straw biochars. *Sci. Total Environ.* **2020**, *699*, 134–262. [CrossRef]
17. Zhang, M.; Shu, L.; Shen, X.; Guo, X.; Tao, S.; Xing, B.; Wang, X. Characterization of nitrogen-rich biomaterial-derived biochars and their sorption for aromatic compounds. *Environ. Pollut.* **2014**, *195*, 84–90. [CrossRef]
18. Zeng, Y.F.; Xue, Y.W.; Long, L.; Yan, J.P. Novel crayfish shell biochar nanocomposites loaded with Ag-TiO2 nanoparticles exhibit robust antibacterial activity. *Water Air Soil Pollut.* **2019**, *230*, 9–15. [CrossRef]
19. Tran, H.N. Comments on "Characterization and adsorption capacity of raw pomegranate peel biosorbent for copper removal". *J. Clean. Prod.* **2017**, *144*, 553–558. [CrossRef]
20. Attallah, M.F.; Rizk, S.E.; Shady, S.A. Separation of ~(152 + 154)Eu,~(90)Sr from radioactive waste effluent using liquid–liquid extraction by polyglycerol phthalate. *Nucl. Sci. Tech.* **2018**, *29*, 84. [CrossRef]
21. Liu, Y.; Chen, R.; Yuan, D.; Liu, Z.; Meng, M.; Wang, Y.; Han, J.; Meng, X.; Liu, F.; Hu, Z.; et al. Thermal-responsive ion-imprinted polymer based on magnetic mesoporous silica SBA-15 for selective removal of Sr(II) from aqueous solution. *Colloid Polym. Sci.* **2014**, *293*, 109–123. [CrossRef]
22. Zhang, N.; Liu, S.; Jiang, L.; Luo, M.; Chi, C.; Ma, J. Adsorption of strontium from aqueous solution by silica mesoporous SBA-15. *J. Radioanal. Nucl. Chem.* **2014**, *303*, 1671–1677. [CrossRef]
23. Youssef, M.A.; Rizk, H.E.; Attallah, M.F. Purification of liquid scintillation waste from binding radionuclides using different adsorbents. *Radiochim. Acta* **2020**, *108*, 879–887. [CrossRef]
24. Kaveeshwar, A.R.; Kumar, P.S.; Revellame, E.D.; Gang, D.D.; Zappi, M.E.; Subramaniam, R. Adsorption properties and mechanism of barium (II) and strontium (II) removal from fracking wastewater using pecan shell based activated carbon. *J. Clean. Prod.* **2018**, *193*, 1–13. [CrossRef]
25. Jang, J.; Miran, W.; Divine, S.D.; Nawaz, M.; Shahzad, A.; Woo, S.H.; Lee, D.S. Rice straw-based biochar beads for the removal of radioactive strontium from aqueous solution. *Sci. Total Environ.* **2017**, *615*, 698–707. [CrossRef]
26. Choi, J.-W.; Cho, S.; Choi, S.-J. Ecofriendly, selective removal of radioactive strontium ions in aqueous solutions using magnetic banana peels. *Sci. Total Environ.* **2021**, *778*, 146327. [CrossRef]
27. Uematsu, Y.; Ogata, F.; Saenjum, C.; Nakamura, T.; Kawasaki, N. Removing Sr(II) and Cs(I) from the Aqueous Phase Using Basil Seed and Elucidating the Adsorption Mechanism. *Sustainability* **2020**, *12*, 2895. [CrossRef]
28. Imessaoudene, D.; Hanini, S.; Bouzidi, A. Biosorption of strontium from aqueous solutions onto spent coffee grounds. *J. Radioanal. Nucl. Chem.* **2013**, *298*, 893–902. [CrossRef]
29. Wang, F.Y.; Wang, H.; Ma, J.W. Adsorption of cadmium(II) ions from aqueous solution by a new low-cost adsorbent-bamboo charcoal. *J. Hazard. Mater.* **2010**, *177*, 300–306. [CrossRef] [PubMed]
30. Pérez-Calixto, M.; Ortega, A.; Garcia-Uriostegui, L.; Burillo, G. Synthesis and characterization of N-vinylcaprolactam/N,N-dimethylacrylamide grafted onto chitosan networks by gamma radiation. *Radiat. Phys. Chem.* **2016**, *119*, 228–235. [CrossRef]
31. Nasef, S.M.; Khozemy, E.E.; Kamoun, E.A.; El-gendi, H. Gamma Radiation-Induced Crosslinked Composite Membranes Based on Polyvinyl Alcohol/Chitosan/$AgNO_3$/Vitamin E for Biomedical Applications. *Int. J. Biol. Macromol.* **2019**, *137*, 878–885. [CrossRef]
32. Swantomo, D.; Basuki, K.T.; Synthesis, S.R. Characterization of Graft Copolymer Rice Straw Cellulose-Acrylamide. *Atom Indones.* **2013**, *39*, 57–64. [CrossRef]
33. Qiu, L.; Feng, J.; Dai, Y.; Chang, S. Biosorption of strontium ions from simulated high-level liquid waste by living Saccharomyces cerevisiae. *Environ. Sci. Pollut. Res.* **2018**, *25*, 17194–17206. [CrossRef]
34. Wang, T.; Zheng, X.; Wang, X.; Lu, X.; Shen, Y. Different biosorption mechanisms of Uranium(VI) by live and heat-killed Saccharomyces cerevisiae under environmentally relevant conditions. *J. Environ. Radioact.* **2017**, *167*, 92–99. [CrossRef] [PubMed]
35. Zhang, X.; Zhang, P.; Yuan, X.; Li, Y.; Han, L. Effect of pyrolysis temperature and correlation analysis on the yield and physicochemical properties of crop residue biochar. *Bioresour. Technol.* **2019**, *296*, 122318. [CrossRef]
36. Lee, X.J.; Lee, L.Y.; Hiew, B.Y.Z.; Gan, S.; Thangalazhy Gopakumar, S.; Kiat Ng, H. Multistage optimizations of slow pyrolysis synthesis of biochar from palm oil sludge for adsorption of lead. *Bioresour. Technol.* **2017**, *245*, 944–953. [CrossRef]
37. Zu, Z. Cationic dyes removal using low-cost banana peel biosorbent. *Am. J. Sci.* **2018**, *8*, 32–38.
38. Mondal, S.; Majumder, S.K. Honeycomb-like porous activated carbon for efficient copper (II) adsorption synthesized from natural source: Kinetic study and equilibrium isotherm analysis. *J. Environ. Chem. Eng.* **2019**, *7*, 103236. [CrossRef]
39. Kearns, J.; Wellborn, L.; Summers, R.; Knappe, D. 2,4-D adsorption to biochars: Effect of preparation conditions on equilibrium adsorption capacity and comparison with commercial activated carbon literature data. *Water Res.* **2014**, *62*, 20–28. [CrossRef]
40. Zhao, L.; Cao, X.; Mašek, O.; Zimmerman, A. Heterogeneity of biochar properties as a function of feedstock sources and production temperatures. *J. Hazard. Mater.* **2013**, *256–257*, 1–9. [CrossRef] [PubMed]
41. Zhao, B.; O'Connor, D.; Zhang, J.; Peng, T.; Shen, Z.; Tsang, D.C.W.; Hou, D. Effect of pyrolysis temperature, heating rate, and residence time on rapeseed stem derived biochar. *J. Clean. Prod.* **2018**, *174*, 977–987. [CrossRef]
42. Chen, Y.; Yang, H.; Wang, X.; Zhang, S.; Chen, H. Biomass-based pyrolytic polygeneration system on cotton stalk pyrolysis: Influence of temperature. *Bioresour. Technol.* **2012**, *107*, 411–418. [CrossRef] [PubMed]

43. Sigmund, G.; Hüffer, T.; Hofmann, T.; Kah, M. Biochar total surface area and total pore volume determined by N_2 and CO_2 physisorption are strongly influenced by degassing temperature. *Sci. Total Environ.* **2017**, *580*, 770–775. [CrossRef] [PubMed]
44. Wang, S.; Bian, S.; Liu, J.; Li, J.; Xu, S.; Liang, Z. Highly adsorptive pristine and magnetic biochars prepared from crayfish shell for removal of Cu(II) and Pb(II). *J. Taiwan Inst. Chem. Eng.* **2021**, *127*, 175–185. [CrossRef]
45. Sun, T.; Xu, Y.; Sun, Y.; Wang, L.; Liang, X.; Jia, H. Crayfish shell biochar for the mitigation of Pb contaminated water and soil: Characteristics, mechanisms, and applications. *Environ. Pollut.* **2020**, *271*, 116308. [CrossRef]
46. Deshmukh, P.D.; Khadse, G.K.; Shinde, V.M.; Labhasetwar, P. Cadmium Removal from Aqueous Solutions Using Dried Banana Peels as An Adsorbent: Kinetics and Equilibrium Modeling. *J. Bioremediation Biodegrad.* **2017**, *8*, 1000395. [CrossRef]
47. Lu, H.; Zhang, W.; Yang, Y.; Huang, X.; Wang, S.; Qiu, R. Relative distribution of Pb^{2+} sorption mechanisms by sludge-derived biochar. *Water Res.* **2012**, *46*, 854–862. [CrossRef]
48. Cao, X.; Harris, W. Properties of dairy-manure-derived biochar pertinent to its potential use in remediation. *Bioresour. Technol.* **2010**, *101*, 5222–5228. [CrossRef]
49. Xia, Y.; Yang, T.; Zhu, N.; Li, D.; Chen, Z.; Lang, Q.; Liu, Z.; Jiao, W. Enhanced adsorption of Pb(II) onto modified hydrochar: Modeling and mechanism analysis. *Bioresour. Technol.* **2019**, *288*, 121593. [CrossRef]
50. Chia, C.H.; Gong, B.; Joseph, S.D.; Marjo, C.E.; Munroe, P.; Rich, A.M. Imaging of mineral enriched biochar by FTIR, Raman and SEM-EDX. *Vib. Spectrosc.* **2012**, *62*, 248–257. [CrossRef]
51. Zhou, L.; Ji, L.; Ma, P.-C.; Shao, Y.; Zhang, H.; Gao, W.; Li, Y. Development of carbon nanotubes/$CoFe_2O_4$ magnetic hybrid material for removal of tetrabromobisphenol A and Pb(II). *J. Hazard. Mater.* **2014**, *265*, 104–114. [CrossRef]
52. Lee, H.-K.; Lee, H.-J.; Choi, J.-W.; Oh, W.; Choi, S.-J. Selective removal of cesium ions from aqueous solutions by zinc hexacyanoferrate functionalized magnetic carbon nanotube composites as adsorbent. *J. Radioanal. Nucl. Chem.* **2017**, *314*, 2357–2363. [CrossRef]
53. Koilraj, P.; Kamura, Y.; Sasaki, K. Synergetic co-immobilization of SeO_4^{2-} and Sr^{2+} from aqueous solution onto multifunctional graphene oxide and carbon-dot based layered double hydroxide nanocomposites and their mechanistic investigation. *J. Mater. Chem. A* **2018**, *6*, 10008–10018. [CrossRef]
54. Thirumavalavan, M.; Lai, Y.-L.; Lee, J.-F. Fourier Transform Infrared Spectroscopic Analysis of Fruit Peels before and after the Adsorption of Heavy Metal Ions from Aqueous Solution. *J. Chem. Eng. Data* **2011**, *56*, 2249–2255. [CrossRef]
55. Liu, M.; Chen, C.; Hu, J.; Wu, X.; Wang, X. Synthesis of Magnetite/Graphene Oxide Composite and Application for Cobalt(II) Removal. *J. Phys. Chem. C* **2011**, *115*, 25234–25240. [CrossRef]
56. Ding, D.; Lei, Z.; Yang, Y.; Feng, C.; Zhang, Z. Selective removal of cesium from aqueous solutions with nickel (II) hexacyanoferrate (III) functionalized agricultural residue–walnut shell. *J. Hazard. Mater.* **2014**, *14*, 2251–2276. [CrossRef] [PubMed]
57. Wang, J.; Guo, X. Adsorption isotherm models: Classification, physical meaning, application and solving method. *Chemosphere* **2020**, *258*, 127–134. [CrossRef] [PubMed]
58. Zhuravlev, I. Titanium Silicates Precipitated on the Rice Husk Biochar as Adsorbents for the Extraction of Cesium and Strontium Radioisotope Ions. *Colloids Interfaces* **2019**, *3*, 36. [CrossRef]
59. Saleh, A.S.; Ibrahim, A.G.; Elsharma, E.M.; Metwally, E.; Siyam, T. Radiation grafting of acrylamide and maleic acid on chitosan and effective application for removal of Co(II) from aqueous solutions. *Radiat. Phys. Chem.* **2018**, *144*, 116–124. [CrossRef]
60. Basuki, K.T.; Swantomo, D.; Sigit; Megasari, K. Effect of Deacetylation on Characterization of pH Stimulus Responsive Chitosan-Acrylamide Hydrogels Using Radiation. *Adv. Mater. Res.* **2014**, *896*, 292–295. [CrossRef]
61. Wang, Y.; Long, J.; Xu, W.; Luo, H.; Liu, J.; Zhang, Y.; Li, J.; Luo, X. Removal of uranium (VI) from simulated wastewater by a novel porous membrane based on crosslinked chitosan, UiO-66-NH 2 and polyvinyl alcohol. *J. Radioanal. Nucl. Chem.* **2021**, *173*, 1142–1159.
62. Mei, J.; Mo, S.; Zhang, H.; Zheng, X.; Li, Z. Removal of Sr(II) from water with highly-elastic carboxymethyl chitosan gel. *Int. J. Biol. Macromol.* **2020**, *163*, 1097–1105. [CrossRef] [PubMed]
63. Yi, R.; Ye, G.; Chen, J. Synthesis of core–shell magnetic titanate nanofibers composite for the efficient removal of Sr(ii). *RSC Adv.* **2019**, *9*, 27242–27249. [CrossRef] [PubMed]
64. Liu, D.; Zheng, H.; Yang, W.; Chen, Y. Efficient removal of Sr(II) from aqueous solution by melamine-trimesic acid modified attapulgite composite. *J. Radioanal. Nucl. Chem.* **2019**, *321*, 97–108. [CrossRef]
65. Chu, Z.C.; Liu, J.H.; Han, C.L. Removal of strontium ions from aqueous solution using hybrid membranes: Kinetics and thermodynamics. *Chin. J. Chem. Eng.* **2015**, *23*, 1620–1626. [CrossRef]
66. Yang, S.; Gao, M.; Luo, Z. Adsorption of 2-Naphthol on the organo-montmorillonites modifified by Gemini surfactants with different spacers. *Chem. Eng. J.* **2014**, *256*, 39–50. [CrossRef]
67. Swantomo, D.; Faturrahman, I.R.; Basuki, K.T.; Wongsawaeng, D. Chitosan-polyacrylamide graft copolymers prepared with gamma irradiation for gold cyanide adsorption. *Polym. Technol. Mater.* **2020**, *59*, 1284–1291. [CrossRef]
68. Cheung, W.; Szeto, Y.; McKay, G. Intraparticle diffusion processes during acid dye adsorption onto chitosan. *Bioresour. Technol.* **2007**, *98*, 2897–2904. [CrossRef]
69. Cordon, M.J.; Vega-Vila, J.C.; Casper, A.; Huang, Z.; Gounder, R. Tighter Confinement Increases Selectivity of D-Glucose Isomerization Toward-L-Sorbose in Titanium Zeolites. *Angew. Chem. Int. Edit.* **2020**, *2020*, 6–12.

70. Vrtoch, M.; Pipíška, M.; Horník, J.; Augustín, J. Lesný, J. Sorption of cesium from water solutions on potassium nickel hexacyanoferrate-modifified Agaricus bisporus mushroom biomass. *J. Radioanal. Nucl. Chem.* **2011**, *287*, 853–862. [CrossRef]
71. Uçak, S.S.; Aydın, A. A novel thiourea derivative for preconcentration of copper(II), nickel(II), cadmium(II), lead(II) and iron(II) from seawater samples for Flame Atomic Absorption Spectrophotometry. *Mar. Pollut. Bull.* **2022**, *180*, 113787. [CrossRef] [PubMed]
72. Hong, H.-J.; Ryu, J.; Park, I.-S.; Ryu, T.; Chung, K.-S.; Kim, B.-G. Investigation of the strontium (Sr(II)) adsorption of an alginate microsphere as a low-cost adsorbent for removal and recovery from seawater. *J. Environ. Manag.* **2016**, *165*, 263–270. [CrossRef] [PubMed]

Disclaimer/Publisher's Note: The statements, opinions and data contained in all publications are solely those of the individual author(s) and contributor(s) and not of MDPI and/or the editor(s). MDPI and/or the editor(s) disclaim responsibility for any injury to people or property resulting from any ideas, methods, instructions or products referred to in the content.